Triangulum II: A Very Metal-poor and Dynamically Hot Stellar System

The Astrophysical Journal, 818:40 (7pp), 2016 February 10 doi:10.3847/0004-637X/818/1/40

TRIANGULUM II: A VERY METAL-POOR AND DYNAMICALLY HOT STELLAR SYSTEM

Nicolas F. Martin[1,2], Rodrigo A. Ibata[1], Michelle L. M. Collins[3,4,10], R. Michael Rich[5], Eric F. Bell[6], Annette M. N. Ferguson[7], Benjamin P. M. Laevens[1,2], Hans-Walter Rix[2], Scott C. Chapman[8], and Andreas Koch[9]
[1] Observatoire astronomique de Strasbourg, Université de Strasbourg, CNRS, UMR 7550, 11 rue de l'Université, F-67000 Strasbourg, France; nicolas.martin@astro.unistra.fr
[2] Max-Planck-Institut für Astronomie, Königstuhl 17, D-69117 Heidelberg, Germany
[3] Astronomy Department, Yale University, New Haven, CT 06520, USA
[4] Department of Physics, University of Surrey, Guildford, GU2 7XH, Surrey, UK
[5] Department of Physics and Astronomy, University of California, Los Angeles, PAB, 430 Portola Plaza, Los Angeles, CA 90095-1547, USA
[6] Department of Astronomy, University of Michigan, 500 Church Street, Ann Arbor, MI 48109, USA
[7] Institute for Astronomy, University of Edinburgh, Royal Observatory, Blackford Hill, Edinburgh EH9 3HJ, UK
[8] Department of Physics and Atmospheric Science, Dalhousie University, Coburg Road, Halifax, NS B3H 1A6, Canada
[9] Landessternwarte, Zentrum für Astronomie der Universität Heidelberg, Königstuhl 12, D-69117 Heidelberg, Germany
Received 2015 October 15; accepted 2015 December 11; published 2016 February 5

ABSTRACT

We present a study of the recently discovered compact stellar system Triangulum II. From observations conducted with the DEIMOS spectrograph on Keck II, we obtained spectra for 13 member stars that follow the CMD features of this very faint stellar system and include two bright red giant branch stars. Tri II has a very negative radial velocity ($\langle v_r \rangle = -383.7^{+3.0}_{-3.3}$ km s^{-1}) that translates to $\langle v_{r,gsr} \rangle \simeq -264$ km s^{-1} and confirms it is a Milky Way satellite. We show that, despite the small data set, there is evidence that Tri II has complex internal kinematics. Its radial velocity dispersion increases from $4.4^{+2.8}_{-2.0}$ km s^{-1} in the central 2′ to $14.1^{+5.8}_{-4.2}$ km s^{-1} outwards. The velocity dispersion of the full sample is inferred to be $\sigma_{vr} = 9.9^{+3.2}_{-2.2}$ km s^{-1}. From the two bright RGB member stars we measure an average metallicity $\langle [Fe/H] \rangle = -2.6 \pm 0.2$, placing Tri II among the most metal-poor Milky Way dwarf galaxies. In addition, the spectra of the fainter member stars exhibit differences in their line widths that could be the indication of a metallicity dispersion in the system. All these properties paint a complex picture for Tri II, whose nature and current state are largely speculative. The inferred metallicity properties of the system however lead us to favor a scenario in which Tri II is a dwarf galaxy that is either disrupting or embedded in a stellar stream.

Key words: galaxies: individual (Tri II) – galaxies: kinematics and dynamics – Local Group

1. INTRODUCTION

A large number of faint and small stellar systems have been uncovered over the last decade thanks to wide photometric surveys. The harvest of such objects, which started with Willman 1 (Willman et al. 2005) and then Segue 1 (Belokurov et al. 2007), blossomed through systematic searches of the Sloan Digital Sky Survey (SDSS; Belokurov et al. 2009) and, more recently, of the Dark Energy Survey (DES; Bechtol et al. 2015; Drlica-Wagner et al. 2015; Koposov et al. 2015) and the Panoramic Telescope and Rapid Response System 1 (Pan-STARRS1; Laevens et al. 2015a, 2015b). The photometric properties of many of these systems ambiguously locate them in a region of parameter space where dwarf galaxies appear to mix with globular clusters (Gilmore et al. 2007). Spectroscopic studies of their stars are therefore unavoidable to show that they are either dynamically cold and display no metallicity dispersion (e.g., Laevens 1; Kirby et al. 2015), as expected for globular clusters, or that they are dynamically hot (e.g., Segue 1; Geha et al. 2009), have a metallicity dispersion (e.g., Segue 2; Kirby et al. 2013a), and/or lie on the luminosity–metallicity relation followed by dwarf galaxies (e.g., Hydra II and Draco II; Kirby et al. 2015; Martin et al. 2015).

Although they are expected by the dozen in simulations (Tollerud et al. 2008; Bullock et al. 2010), only a handful of these faint and small stellar systems have so far been confirmed as dwarf galaxies. Any new addition to the list is particularly valuable as these objects are among the most promising for the indirect detection of the elusive dark matter particle (e.g., Geringer-Sameth et al. 2015). Their small baryonic component ($L \sim 10^{2-4}\,L_\odot$) makes them hard to find and study but, at the same time, gives powerful insight into the interplay of physical processes that drive galaxy formation at low masses and in shallow potential wells. The characterization of these systems is, however, made difficult by the potential presence of binary stars that can significantly inflate the intrinsic velocity dispersion of a system with a velocity dispersion of only a few km s^{-1} (McConnachie & Côté 2010). In addition, the usual assumption of dynamical equilibrium can be inappropriate for systems that are often found within ∼40 kpc of the Galactic center, further impeding their study (e.g., Willman 1; Willman et al. 2011). Finally, the difficulty to disentangle member stars from foreground contamination can sometimes further compound the analysis of these faint objects (e.g., Bonnivard et al. 2015).

In this paper, we report a spectroscopic study of the Triangulum II (Tri II) stellar system discovered by Laevens et al. (2015b) in Pan-STARRS1 and confirmed with deep Large Binocular Camera (LBC) photometry. Tri II is very faint ($M_V = -1.8 \pm 0.5$), fairly compact ($r_h = 34^{+9}_{-8}$ pc), and located at 30 ± 2 kpc from the Sun, or 36 ± 2 kpc from the Galactic center. So far as one can infer from the photometry, it appears to contain only old and metal-poor stars.

We present the Keck II/DEIMOS data used for the analysis in Section 2 of this paper, the results of the spectroscopic study in Section 3, while Section 4 is devoted to a discussion on our findings.

[10] Hubble Fellow

2. OBSERVATIONS AND DATA

Two masks targeting Tri II potential member stars were observed during the night of 2015 September 17, with the DEep Imaging Multi-Object Spectrograph (DEIMOS) on Keck II (Faber et al. 2003) under reasonably good conditions (0.″7–1.″0 seeing and ∼60% humidity; PI: Rich, program ID: 2015B_U064D). The LBC photometry used by Laevens et al. (2015b) to confirm the discovery of the satellite was used to place slits on stars selected in the color–magnitude diagram (CMD) to follow the system's main sequence turn off (MSTO), sub-giant branch (SGB), and red giant branch (RGB). The selection was purposefully tight around the sharp MSTO and loose around the RGB region that cannot be selected out of the MW foreground contamination from the photometry alone.

Each mask was integrated for 3600 s, split into three sub-exposures for cosmic-ray removal. The spectrograph was set up with the 1200 lines/mm grating, which translates to ∼0.33 Å per pixel in the calcium II triplet (CaT) region we focus on. The full spectra cover the range 6600–9400 Å. Raw frames are processed through our own pipeline, which we developed over the years to specifically reduce DEIMOS spectra. We refer the reader to Ibata et al. (2011) for an overview of the details of the processing and the results of using the pipeline on high quality data. Briefly, the reduction method calibrates each pixel of the original spectroscopic frame in both wavelength and spatial position on the sky. In this way the data retain their original pixel binning, and one avoids introducing the correlated noise that occurs when spectra are extracted and co-added. The wavelength solution is given by a fit to arc-lamp frames taken immediately after the science frames. We also allow for a wavelength re-calibration using the Fraunhofer A band in the range 7595–7630 Å in order to perform small telluric corrections when the signal to noise of the spectra is sufficient. A two-dimensional sky spectrum model is built for each slitlet following a procedure inspired by the method of Kelson (2003). Finally, the radial velocity (and corresponding uncertainty) of the target stars is measured by fitting a simple Gaussian model of the Ca II triplet lines to the pixel data minus the sky spectrum. Only stars with large enough signal-to-noise ratio (S/N > 3 per pixel) and velocity uncertainties lower than 15 km s^{-1} are kept for the analysis, leaving a total sample of 50 stars.

Velocity uncertainties measured by the pipeline are known not to fully account for low level systematics. Following Ibata et al. (2011), we add an uncertainty floor of 2.25 km s^{-1} in quadrature to the velocity uncertainties measured directly from the spectra. Finally, we measure the equivalent widths of the CaT lines and their uncertainties by independently fitting to the three lines Moffat functions shifted to the velocity of a given star (Ibata et al. 2005).

Unless specified otherwise, radial velocities reported in this paper are heliocentric velocities, corrected for the motion of the Earth around the Sun, but not corrected for solar motion. The known and derived properties of Tri II are summarized in Table 1 and the properties of the spectroscopic sample stars are listed below in Table 2.

Table 1
Properties of Tri II

RA[a] (ICRS)	02:13:17.4
Dec[a] (ICRS)	+36:10:42.4
Heliocentric distance[a] (kpc)	30 ± 2
Galactocentric distance[a] (kpc)	36 ± 2
r_h[a] (′)	$3.9^{+1.1}_{-0.9}$
r_h[a] (pc)	34^{+9}_{-8}
M_V[a]	−1.8 ± 0.5
L_V ($L_\odot$)[a]	$10^{2.6\pm0.2}$
	Global kinematics
$\langle v_r \rangle$ (km s^{-1})	$-383.7^{+3.0}_{-3.3}$
$\langle v_{r,gsr} \rangle$ (km s^{-1})	−264
σ_{vr} (km s^{-1})	$9.9^{+3.2}_{-2.2}$
	Inner kinematics (<2′)
$\langle v_r \rangle$ (km s^{-1})	$-379.8^{+2.1}_{-2.7}$
σ_{vr} (km s^{-1})	$4.4^{+2.8}_{-2.0}$
	Outer kinematics (>2′)
$\langle v_r \rangle$ (km s^{-1})	$-387.3^{+5.7}_{-6.3}$
σ_{vr} (km s^{-1})	$14.1^{+5.8}_{-4.2}$
⟨[Fe/H]⟩	−2.6 ± 0.2

Note.
[a] From Laevens et al. (2015b).

3. ANALYSIS

3.1. Velocities

Stars with good quality spectra are displayed in Figure 1 over the CMD of Tri II in the left-hand panel and over the spatial distribution of possible Tri II stars in the right-hand panel. A group of stars with highly negative velocities, shown in dark blue, is almost perfectly aligned with the favored old and metal-poor isochrone of Laevens et al. (2015b, 13 Gyr and [Fe/H] = −2.2). Most of these stars are MSTO or SGB stars but the sample also contains two RGB stars that shall prove valuable in deriving the metallicity of Tri II. A large fraction of the stars with very negative velocities is also concentrated within the half-light radius of Tri II represented by the blue ellipse, even though some member stars are also located beyond and throughout the region covered by the DEIMOS masks.

The velocity distribution of the sample stars shown in the top panel of Figure 2 reveals the velocity peak produced by Tri II stars. Located around $v_r \sim -385$ km s^{-1}, it appears completely isolated from the MW foreground contamination and confirms that all stars shown in dark blue in Figure 1 are member stars. The velocity peak is also surprisingly wide. Fitting a Gaussian distribution to the 13 member stars corroborates this first impression as we infer a velocity dispersion of $\sigma_{vr} = 9.9^{+3.2}_{-2.2}$ km s^{-1} around a systemic velocity of $\langle v_r \rangle = -383.7^{+3.0}_{-3.3}$ km s^{-1} (see the bottom panels of Figure 2 for the parameters' probability distribution functions or pdfs). Such a value is at odds with velocity dispersion measurements usually obtained in similarly faint and compact MW systems. Recent studies consistently infer values of, at most, a few km s^{-1} (Martin et al. 2007a; Simon & Geha 2007; Geha et al. 2009; Willman et al. 2011; Kirby et al. 2013b, 2015; Martin et al. 2015).

Figure 3 shows, however, that the radial velocities of member stars appear to flare up with distance from the center of the system. The central half of the sample is much more closely aligned in velocity than its outer half. Fitting the velocity distribution for the six member stars within 2′ yields

Table 2
Properties of Observed Stars Meeting the Quality Criteria

#	R.A. (ICRS)	decl. (ICRS)	R^a (′)	g_{P1}	i_{P1}	v_r (km s^{-1})	δ_{vr} (km s^{-1})	S/N (per pixel)	Member?	EW_{2+3} (Å)	[Fe/H]
1	33.1946678	36.1328316	6.8	19.955	19.347	−90.6	2.8	23.2	N	⋯	⋯
2	33.2111244	36.1401672	5.9	20.006	19.410	−99.3	2.6	13.2	N	⋯	⋯
3	33.4113731	36.2505836	6.1	20.026	19.375	−76.8	2.6	15.5	N	⋯	⋯
4	33.3050842	36.1931953	1.2	20.092	19.578	−276.2	2.9	13.4	N	⋯	⋯
5	33.3774185	36.2628899	5.7	20.344	19.702	−83.2	2.8	12.0	N	⋯	⋯
6	33.3839149	36.2578049	5.6	20.658	20.168	−111.7	3.8	7.3	N	⋯	⋯
7	33.3341675	36.2451935	4.0	20.799	20.253	−97.3	3.5	7.1	N	⋯	⋯
8	33.2591667	36.2090836	3.6	21.165	20.737	−387.1	7.7	4.9	Y	⋯	⋯
9	33.3639183	36.2251930	3.4	21.499	21.158	−404.7	5.1	3.8	Y	⋯	⋯
10	33.4349174	36.3003044	9.1	20.180	19.403	−42.2	4.1	7.0	N	⋯	⋯
11	33.3940010	36.2913055	7.6	21.106	20.682	−78.6	4.6	4.8	N	⋯	⋯
11	33.3940010	36.2913055	7.6	21.101	20.714	−78.6	4.6	4.8	N	⋯	⋯
12	33.2499161	36.1958885	3.7	18.036	17.258	−80.8	2.3	48.1	N	⋯	⋯
13	33.2220421	36.1532211	5.1	19.294	18.586	−172.5	2.4	26.5	N	⋯	⋯
14	33.2612076	36.1757774	3.0	19.427	18.863	−46.2	2.5	19.4	N	⋯	⋯
15	33.3087502	36.2062492	1.8	17.416	16.429	1.3	2.3	54.4	N	⋯	⋯
16	33.3540840	36.2714462	5.8	17.152	16.330	−13.7	2.3	67.3	N	⋯	⋯
17	33.3997078	36.2773628	7.0	18.224	17.460	−78.8	2.3	45.1	N	⋯	⋯
18	33.4496231	36.2708626	8.3	19.047	18.278	−152.4	2.6	17.8	N	⋯	⋯
19	33.3174171	36.1878624	0.6	19.387	18.731	−59.7	2.4	22.2	N	⋯	⋯
20	33.3305016	36.1926117	0.9	20.565	19.907	−378.7	2.9	11.7	Y	1.41 ± 0.21	−2.3 ± 0.2
21	33.3165016	36.1710815	0.5	20.667	20.059	−382.8	3.1	10.8	Y	0.87 ± 0.20	−3.0 ± 0.6[b]
22	33.3029175	36.1470566	2.1	20.957	20.458	−387.0	3.8	7.6	Y	⋯	
23	33.3359184	36.1629181	1.1	21.109	20.562	−387.9	3.6	7.1	Y	⋯	⋯
24	33.3416672	36.1738892	1.0	21.552	21.222	−383.1	4.9	5.3	Y	⋯	⋯
25	33.3214149	36.1205826	3.5	21.568	21.196	−362.8	5.6	4.5	Y	⋯	⋯
26	33.3535004	36.1727219	1.5	21.799	21.398	−84.1	8.2	3.5	N	⋯	⋯
27	33.3389587	36.1414452	2.4	21.814	21.458	−401.4	6.6	4.2	Y	⋯	⋯
28	33.3247490	36.1699982	0.5	21.991	21.616	366.6	6.9	3.5	N	⋯	⋯
29	33.3789597	36.1988907	3.0	22.326	21.877	−397.1	7.8	3.1	Y	⋯	⋯
30	33.4619598	36.2307205	7.4	20.690	20.180	−215.8	2.9	11.2	N	⋯	⋯
31	33.4694176	36.2234154	7.6	20.845	20.223	−375.8	3.1	9.8	Y	3.90 ± 0.45	−0.7 ± 0.2[b]
32	33.4769173	36.2040291	7.6	21.132	20.700	−225.9	3.5	6.8	N	⋯	⋯
33	33.2707901	36.0966949	5.5	17.659	16.706	−14.2	2.4	53.3	N	⋯	⋯
34	33.2869987	36.0956383	5.3	18.630	18.031	−43.1	2.4	31.0	N	⋯	⋯
35	33.2285843	36.1292763	5.4	17.306	16.496	−44.7	2.3	60.3	N	⋯	⋯
36	33.2309570	36.1342239	5.2	19.463	18.691	−1.2	2.4	21.5	N	⋯	⋯
37	33.2211685	36.1413040	5.4	17.928	17.216	−44.2	2.3	46.5	N	⋯	⋯
38	33.4219170	36.1992760	5.0	17.195	16.231	10.8	2.3	78.9	N	⋯	⋯
39	33.4609985	36.1992493	6.8	16.906	16.181	−30.1	2.4	57.1	N	⋯	⋯
40	33.3189583	36.1793900	0.2	17.585	16.692	−379.2	2.3	73.3	Y	1.79 ± 0.05	−2.6 ± 0.1
41	33.3302078	36.1485825	1.8	17.699	16.858	−23.2	2.3	54.9	N	⋯	⋯
42	33.3511658	36.1708603	1.5	17.561	16.772	−11.7	2.3	57.2	N	⋯	⋯
43	33.4364586	36.2213593	6.1	18.337	17.426	−93.3	2.3	39.8	N	⋯	⋯
44	33.3328743	36.2034149	1.6	18.925	18.122	−173.5	4.8	30.0	N	⋯	⋯
45	33.3890419	36.1674995	3.3	19.115	18.539	−59.2	2.4	25.2	N		
46	33.3397484	36.1659431	1.1	19.286	18.540	−372.5	2.4	26.4	Y	1.33 ± 0.08	−2.6 ± 0.1
47	33.3222084	36.1384430	2.4	19.019	18.452	−71.4	2.4	25.7	N	⋯	⋯
48	33.3827095	36.2173882	3.7	17.149	16.205	17.3	2.3	70.2	N	⋯	⋯
49	33.4824982	36.2344437	8.4	17.344	16.462	2.8	2.3	61.6	N	⋯	⋯
50	33.4132080	36.1776123	4.4	19.096	18.472	−27.4	2.4	26.9	N	⋯	⋯

Notes.
[a] Distance from Tri II's centroid.
[b] These stars are fainter than the magnitude range over which the Starkenburg et al. (2010) relation was calibrated; their [Fe/H] measurements should therefore be taken with caution.

$\langle v_r \rangle = -379.8^{+2.1}_{-2.7}$ km s^{-1} and $\sigma_{vr} = 4.4^{+2.8}_{-2.0}$ km s^{-1}, whereas the outermost seven stars yield $\langle v_r \rangle = -387.3^{+5.7}_{-6.3}$ km s^{-1} and $\sigma_{vr} = 14.1^{+5.8}_{-4.2}$ km s^{-1}. While the systemic velocities of the inner and outer samples are compatible, this is hardly the case for the velocity dispersion measurements (see pdfs in the bottom panels of Figure 2). Although we cannot completely rule out the compatibility of the two measurements inferred from a small number of stars in both samples, we find that the velocity dispersions are nevertheless discrepant at the 2σ level, confirming the visual impression from Figure 3.

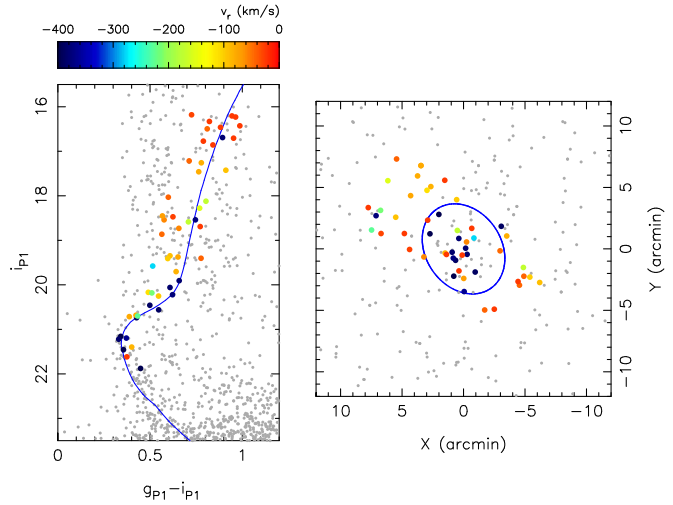

Figure 1. Left: LBC CMD of stars within $2r_h$ of Tri II's centroid. Stars with spectra that passed our quality cuts are shown color-coded by velocity whereas stars without spectroscopic information are represented by gray dots. The 13 Tri II member stars appear as dark blue points with large negative velocities and follow the Parsec isochrone (Bressan et al. 2012) shown in blue, favored by Laevens et al. (2015b) to reproduce the CMD features of the stellar system (13 Gyr and [Fe/H] = −2.2). Right: distribution of the LBC stars selected to follow the Tri II CMD features. The color-coding is the same as in the left-hand panel. The blue ellipse represents the region within the half-light radius of Tri II.

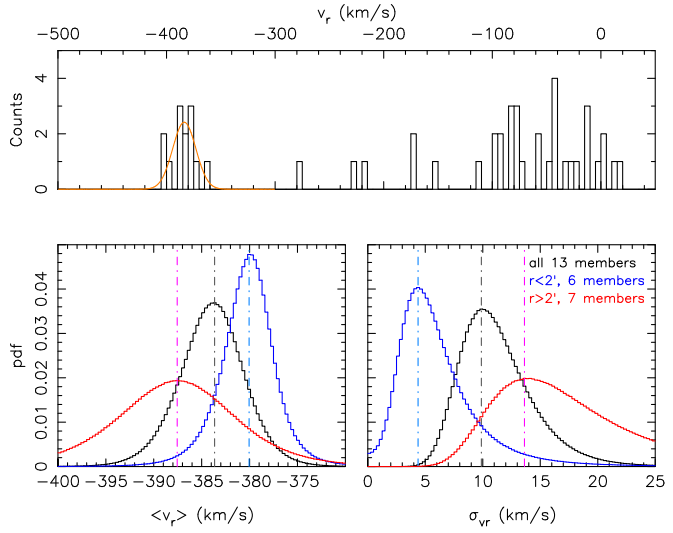

Figure 2. Top: heliocentric velocity distribution of the spectroscopic sample. The velocity peak of Tri II stars is visible at $v_r \sim -385$ km s^{-1}, separated from the MW contamination with $v_r > -300$ km s^{-1}. The orange line displays the best fit to the velocity distribution of Tri II stars, convolved by the median velocity uncertainty. Bottom: pdfs of the systemic velocity (left) and velocity dispersion (right) of the full Tri II sample (black histograms). The blue and red histograms correspond to the pdfs for the inner and outer half of the sample, respectively. The vertical lines indicate the modes of the distributions. Note the discrepant velocity dispersion pdfs for the inner and outer samples.

The large velocity dispersion of the outer sample is robust to the velocity uncertainties as it remains present, even if we increase the uncertainty floor to the unlikely value of 4 km s^{-1}. We also checked for the presence of a velocity gradient as a function of position that could artificially give the impression of the flaring from stars with significantly different velocities on opposite sides of the system. No such gradient was found in the data.

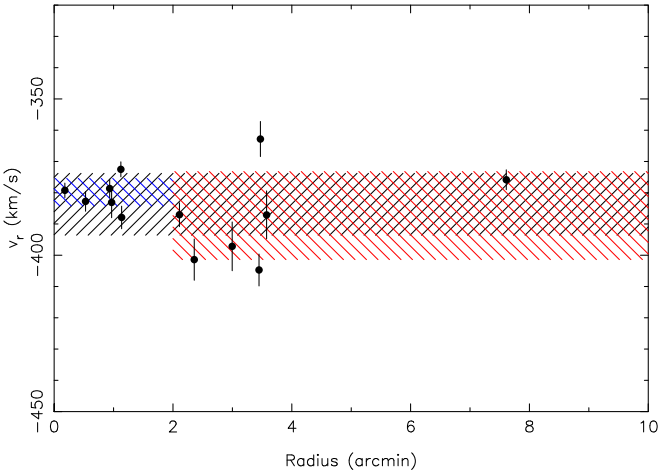

Figure 3. Velocities of Tri II member stars as a function of their distance from the system's centroid, showing an apparent flaring of the radial velocity distribution with distance. The hashed regions correspond to the velocities within $\pm\sigma_{vr}$ for the full sample (gray), the inner sample (blue), and the outer sample (red).

3.2. Metallicities

Two of the observed member stars (stars 40 & 46 in Table 2) are RGB stars bright enough to allow for a determination of their [Fe/H] metallicity via a measure of the equivalent widths of the CaT lines. Starkenburg et al. (2010) have calibrated the relation between the equivalent widths of the second and third CaII lines, EW_{2+3}, down to very low metallicities ($-4.0 <$ [Fe/H] < -0.5). We first convert the i_{P1} magnitudes of the two stars to I_c magnitudes with the Tonry et al. (2012) color equation and, using the Starkenburg et al. (2010) relation, we calculate [Fe/H] $= -2.6 \pm 0.1$ for both RGB stars. These very low metallicity values are confirmed by the inspection of the spectra (top two panels of Figure 4) that both exhibit very weak CaT lines. Assuming a Gaussian metallicity distribution function, we infer a mean metallicity $\langle$[Fe/H]$\rangle = -2.6 \pm 0.2$ for Tri II, which is therefore among the most metal-poor MW satellites.

It is harder to provide a definite conclusion on the presence or absence of a metallicity dispersion in Tri II since two stars alone cannot rule out the presence of a dispersion, even if they are measured to have the same metallicity. Moreover, the other observed member stars are located far below the horizontal branch of the system and the horizontal branch marks the faint limit to which the Starkenburg et al. (2010) relation has been calibrated. Finally, directly extracting a measure of Fe line strengths from DEIMOS spectra with S/N $\lesssim 10$ is fraught with peril.

We note however that the three Tri II stars above the SGB that have similar colors ($g_{P1} - i_{P1} \sim 0.65$), magnitudes ($i_{P1} \sim 20.1$), and signal-to-noise ratio (S/N ~ 10) have inconsistent equivalent widths with $EW_{2+3} = 1.41 \pm 0.21$Å, 0.87 ± 0.20 Å, and 3.90 ± 0.45 Å from the brighter to the fainter star (stars # 20, 21, and 31 from Table 2, respectively). Moreover, none of these stars show strong NaI doublet lines (8183 and 8192 Å) that would indicate that they are foreground contaminants. These EW_{2+3} differences are directly visible on the spectra (lower three panels of Figure 4) and could be interpreted as evidence for a metallicity dispersion in Tri II.

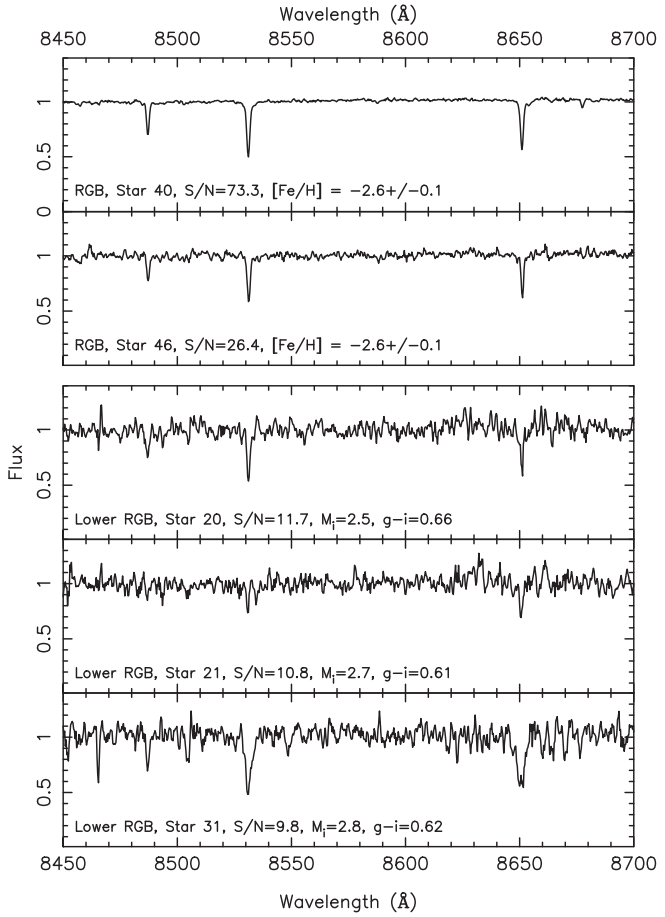

Figure 4. Smoothed spectra of two Tri II RGB (top) and three lower-RGB/SGB member stars in the region around the CaT. The spectra are smoothed with a three-pixel boxcar filter. The properties of the stars are listed in each panel. Note the weak lines of the two RGB stars and the varying line widths of the three lower-RGB/SGB stars that share similar photometric properties, indicating a potential metallicity dispersion in the system.

Blindly applying the Starkenburg et al. (2010) relation for these stars that are fainter than the magnitude range over which it was calibrated[11] yields tentative metallicities of $[\mathrm{Fe/H}] = -2.3 \pm 0.2$, -3.0 ± 0.6, and -0.7 ± 0.2, respectively. From the five brightest confirmed Tri II members, we infer $\langle[\mathrm{Fe/H}]\rangle = -2.2^{+0.4}_{-0.3}$ and a large metallicity dispersion of ∼0.8 dex. We nevertheless stress that direct [Fe/H] measurements are needed from higher S/N spectra to bolster this marginal conclusion.

4. DISCUSSION

We obtained spectra for 13 member stars in the very faint MW satellite Tri II. These stars follow the CMD features of the stellar system and include mainly MSTO and SGB stars, as well as two bright RGB stars. With $\langle v_r \rangle = -383.7^{+3.0}_{-3.3}$ km s^{-1}, Tri II has a very negative radial velocity that translates to $\langle v_{r,gsr} \rangle \simeq -264$ km s^{-1}. We have further shown that, as far as we can tell from only 13 member stars, the internal kinematics of Tri II appear complex, with evidence for a radial velocity dispersion increase from $4.4^{+2.8}_{-2.0}$ km s^{-1} in the central 2′ to $14.1^{+5.8}_{-4.2}$ km s^{-1} outwards. The velocity dispersion of the full sample is inferred to be $\sigma_{vr} = 9.9^{+3.2}_{-2.2}$ km s^{-1}. Finally, the two bright RGB member stars are both measured to have $[\mathrm{Fe/H}] = -2.6 \pm 0.1$ and point to Tri II being among the most metal-poor MW satellites. The spectra of fainter member stars exhibit differences in their line widths that could be due to a metallicity dispersion in the system.

At the distance of Tri II (36 ± 2 kpc from the Galactic center), such a fast infalling velocity is not unexpected for a satellite bound to the MW. It does, however, rule out any association with the numerous stellar structures found nearby in the Milky Way halo. TriAnd (Rocha-Pinto et al. 2004), TriAnd 2 (Martin et al. 2007b), or the PAndAS MW stream (Martin et al. 2014) all have positive $v_{r,gsr}$ (Deason et al. 2014). Tri II is also unrelated to the Segue 2 satellite that is located only ∼10 kpc away but has a very different velocity ($\langle v_r \rangle = -39.2 \pm 2.5$ km s^{-1}; Belokurov et al. 2009).

But what is the nature of Tri II? Taken at face value, the large global velocity dispersion, the very low metallicity, and the potential metallicity dispersion seem to point toward Tri II being a dwarf galaxy rather than a globular cluster. However, the complex kinematics of the system question the assumption of dynamical equilibrium that is required to translate a large velocity dispersion into a large mass and mass-to-light ratio.

Can [Fe/H] *discriminate between globular cluster and dwarf galaxy?* Irrespective of its velocity dispersion, Tri II is among the most metal-poor systems known. No globular cluster is known with a metallicity below $[\mathrm{Fe/H}] = -2.4$ (Harris 1996) and only the Segue 1, Bootes II, and Reticulum II dwarf galaxies, with whom Tri II shares many similar properties (total luminosity, size, distance), are as metal-poor with $[\mathrm{Fe/H}] = -2.7 \pm 0.4$ (Norris et al. 2010) or $[\mathrm{Fe/H}] \sim -2.5$ (Simon et al. 2011) for Segue 1, $[\mathrm{Fe/H}] = -2.9 \pm 0.2$ (Koch & Rich 2014) for Bootes II, and $[\mathrm{Fe/H}] = -2.65 \pm 0.07$ (Simon et al. 2015) or $[\mathrm{Fe/H}] = -2.6 \pm 0.3$ (Walker et al. 2015) for Reticulum II. Figure 5 shows that Tri II is in agreement with the dwarf galaxy metallicity–luminosity relation of Kirby et al. (2013b), even if we include the three stars with tentative metallicity measurements for the inference of the mean metallicity (hollow red square). By analogy, the metallicity of the system therefore appears to favor the dwarf galaxy hypothesis, which would be bolstered further by the marginal evidence of a metallicity dispersion.

What is the dynamical mass of Tri II? It is hard to tell if one takes the increase in the velocity dispersion with radius as a sign that the system is out of equilibrium. On the other hand, if one assumes that the change in σ_{vr} is an (unlikely 2σ) statistical fluctuation and that the global velocity dispersion measured at $\sigma_{vr} = 9.9^{+3.2}_{-2.2}$ km s^{-1} is representative of the true properties of Tri II, one can easily note that it is a significant outlier among other dwarf galaxies of this size, as displayed in Figure 6. Equation (1) of Wolf et al. (2010) relates the mass within the three-dimensional half-light radius, $M_{1/2}$, to the half-light radius and velocity dispersion of a bound system in equilibrium and, in the case of Tri II, yields $M_{1/2} \sim 3 \times 10^6\, M_\odot$ and $(M/L)_{1/2} \sim$ 15,500 in solar units. It would mean that Tri II is almost an order of magnitude more massive than Segue 1 or Reticulum II and, by a wide margin, the most dark matter system known in the universe. Such a large mass seems very improbable.

Could MW contaminants pollute the velocity peak? This also appears unlikely as the inflated velocity dispersion in the

[11] However, see Leaman et al. (2013) and their study of the metal-poor globular cluster M15 for which the calibration is shown to hold ∼2 magnitudes below this system's horizontal branch.

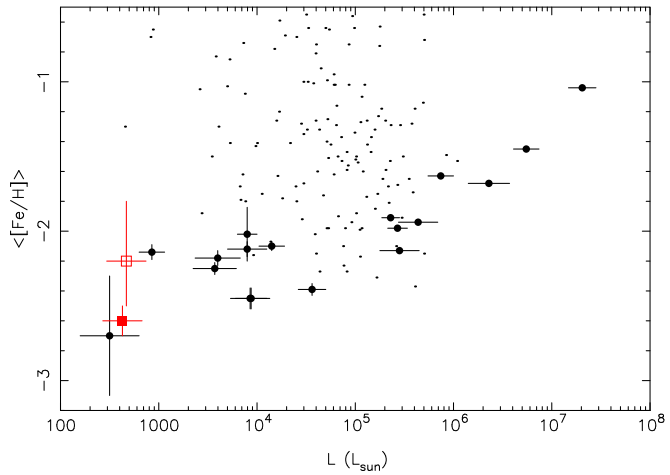

Figure 5. Distribution of MW satellites in the mean metallicity vs. luminosity plane. Large black points correspond to MW dwarf galaxies, as listed in Kirby et al. (2013b), supplemented by Norris et al. (2010), Kirby et al. (2015), and Simon et al. (2015). MW globular clusters are shown as small black dots (Harris 1996). The red squares corresponds to the Tri II measurements, with the filled square representing the inference from the two robust individual stellar metallicities (stars 40 and 46) while the hollow circle corresponds to the inference from the five stars shown in Figure 4 (the two Tri II points have been slightly offset from each other along the luminosity axis so their error bars do not overlap). Both measurements compare well with those of other MW dwarf galaxies.

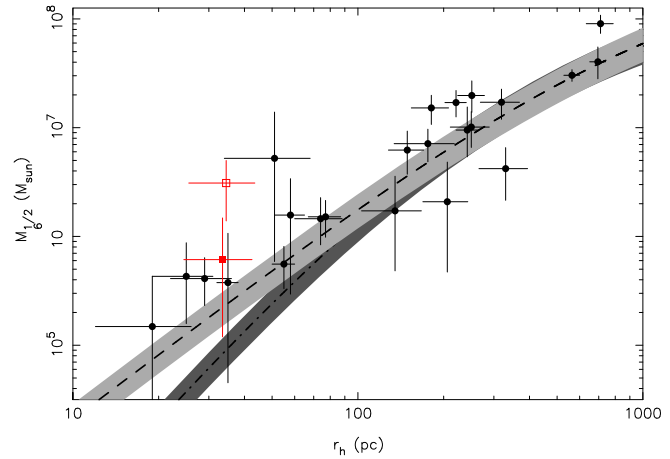

Figure 6. Distribution of MW dwarf galaxies in the r_h–σ_{vr} plane, compared to the Local Group dwarf galaxy mass profiles. The black dashed and dot-dashed lines correspond to the favored Local Group mass profiles of Collins et al. (2014) for a cored or NFW model, respectively, and the gray bands represent the model dispersions determined by these authors. Black points correspond to Milky Way dwarf galaxies, as listed in McConnachie (2012), Kirby et al. (2015), Martin et al. (2015), and Simon et al. (2015). The Tri II data point is shown as a hollow square for the global kinematics determined in this paper, or as a filled square when using the kinematics of the inner sample. The former is a strong outlier whereas the latter fits well with other MW dwarf galaxies. The two Tri II points have been slightly offset from each other along the r_h axis so their error bars do not overlap.

outskirts of Tri II is not driven by any single outlier (see Figure 3). The very negative systemic velocity of Tri II also means it is improbable for the spectroscopic data set to contain more than a single contaminating halo star, if any.

Is Tri II disrupting and/or embedded in a stellar stream? After ruling out that Tri II is in equilibrium or contaminated by MW halo stars, the most likely hypothesis is that the observed increase in the velocity dispersion with radius is genuine. The large velocity dispersion beyond 2′ would then be produced by stars that are not bound to the body of the satellite. This seems at odds with the current measure of the half-light radius of Tri II ($r_{\rm h} = 3.9^{+1.1}_{-0.9}$′; Laevens et al. 2015b), but this measure could be systematically biased by the comparatively small LBC field of view (Muñoz et al. 2012). In fact, the spatial distribution of possible satellite member stars exhibits what could be a more compact central core within ∼2′ surrounded by a more diffuse component (see the right-hand panel of Figure 1 from Laevens et al. 2015b). Upcoming wider and deeper photometric data will allow us to robustly investigate this morphology.

If this ∼2′ core really is the true extent of the main body of Tri II, the velocity dispersion we measure from the inner half of the spectroscopic sample ($\sigma_{\rm vr} = 4.4^{+2.8}_{-2.0}$ km s^{-1}) would be more representative of the satellite's intrinsic properties and would yield a consistent picture with the very faint dwarf galaxies Segue 1 (Simon et al. 2011), Reticulum II (Simon et al. 2015; Walker et al. 2015), or Draco II (Martin et al. 2015), as can be seen in Figure 6. The only conundrum would then be whether Tri II is disrupted by tidal interactions with the Milky Way, or if it is in equilibrium but embedded in a stellar stream. Such a stellar stream could, for instance, be produced by a potentially more massive dwarf galaxy it would have been a satellite of in the past (e.g., Wheeler et al. 2015). The large negative velocity of the system however likely rules out a system that has just now been tidally disrupted after a pericentric passage. The fact that the star with the most discrepant spectrum among those shown in Figure 4 (star 31) is also the only one beyond 2′ could point toward the latter hypothesis but this is hardly conclusive.

At the moment, the puzzling properties of Tri II mean that its nature and current state are largely speculative. We favor the scenario in which Tri II is a dwarf galaxy that is either disrupting or embedded in a stellar stream but cannot completely rule out that it could be a disrupting globular cluster. Whatever the true nature of the satellite, it exhibits unexpected properties that make it very exciting and call for more observations to understand its complexity.

B.P.M.L. acknowledges funding through a 2012 Strasbourg IDEX (Initiative d'Excellence) grant, awarded by the University of Strasbourg. N.F.M. and B.P.M.L. gratefully acknowledge the CNRS for support through PICS project PICS06183. H.-W.R. acknowledges support by the DFG through the SFB 881 (A3). M.L.M.C. acknowledges financial support from the European Research Council (ERC-StG-335936) and from NASA through Hubble Fellowship grant #51337 awarded by the Space Telescope Science Institute, which is operated by the Association of Universities for Research in Astronomy, Inc., for NASA, under contract NAS 5-26555.

The data presented herein were obtained at the WM Keck Observatory, which is operated as a scientific partnership among the California Institute of Technology, the University of California and the National Aeronautics and Space Administration. The Observatory was made possible by the generous financial support of the WM Keck Foundation. The authors wish to recognize and acknowledge the very significant cultural role and reverence that the summit of Mauna Kea has always had within the indigenous Hawaiian community. We are most fortunate to have the opportunity to conduct observations from this mountain.

REFERENCES

Bechtol, K., Drlica-Wagner, A., Balbinot, E., et al. 2015, ApJ, 807, 50
Belokurov, V., Walker, M. G., Evans, N. W., et al. 2009, MNRAS, 397, 1748
Belokurov, V., Zucker, D. B., Evans, N. W., et al. 2007, ApJ, 654, 897
Bonnivard, V., Combet, C., Daniel, M., et al. 2015, MNRAS, 453, 849
Bressan, A., Marigo, P., Girardi, L., et al. 2012, MNRAS, 427, 127
Bullock, J. S., Stewart, K. R., Kaplinghat, M., Tollerud, E. J., & Wolf, J. 2010, ApJ, 717, 1043
Collins, M. L. M., Chapman, S. C., Rich, R. M., et al. 2014, ApJ, 783, 7
Deason, A. J., Belokurov, V., Hamren, K. M., et al. 2014, MNRAS, 444, 3975
Drlica-Wagner, A., Bechtol, K., Rykoff, E. S., et al. 2015, ApJ, 813, 109
Faber, S. M., Phillips, A. C., Kibrick, R. I., et al. 2003, Proc. SPIE, 4841, 1657
Geha, M., Willman, B., Simon, J. D., et al. 2009, ApJ, 692, 1464
Geringer-Sameth, A., Koushiappas, S. M., & Walker, M. G. 2015, PhRvD, 91, 083535
Gilmore, G., Wilkinson, M. I., Wyse, R. F. G., et al. 2007, ApJ, 663, 948
Harris, W. E. 1996, AJ, 112, 1487
Ibata, R., Chapman, S., Ferguson, A. M. N., et al. 2005, ApJ, 634, 287
Ibata, R., Sollima, A., Nipoti, C., et al. 2011, ApJ, 738, 186
Kelson, D. D. 2003, PASP, 115, 688
Kirby, E. N., Boylan-Kolchin, M., Cohen, J. G., et al. 2013a, ApJ, 770, 16
Kirby, E. N., Cohen, J. G., Guhathakurta, P., et al. 2013b, ApJ, 779, 102
Kirby, E. N., Simon, J. D., & Cohen, J. G. 2015, ApJ, 810, 56
Koch, A., & Rich, R. M. 2014, ApJ, 794, 89
Koposov, S. E., Belokurov, V., Torrealba, G., & Wyn Evans, N. 2015, arXiv:1503.02079
Laevens, B. P. M., Martin, N. F., Bernard, E. J., et al. 2015a, ApJ, 813, 44
Laevens, B. P. M., Martin, N. F., Ibata, R. A., et al. 2015b, ApJL, 802, L18
Leaman, R., Venn, K. A., Brooks, A. M., et al. 2013, ApJ, 767, 131
Martin, N. F., Geha, M., Ibata, R. A., et al. 2015, arXiv:1510.01326
Martin, N. F., Ibata, R. A., Chapman, S. C., Irwin, M., & Lewis, G. F. 2007a, MNRAS, 380, 281
Martin, N. F., Ibata, R. A., & Irwin, M. 2007b, ApJL, 668, L123
Martin, N. F., Ibata, R. A., Rich, R. M., et al. 2014, ApJ, 787, 19
McConnachie, A. W. 2012, AJ, 144, 4
McConnachie, A. W., & Côté, P. 2010, ApJL, 722, L209
Muñoz, R. R., Padmanabhan, N., & Geha, M. 2012, ApJ, 745, 127
Norris, J. E., Wyse, R. F. G., Gilmore, G., et al. 2010, ApJ, 723, 1632
Rocha-Pinto, H. J., Majewski, S. R., Skrutskie, M. F., Crane, J. D., & Patterson, R. J. 2004, ApJ, 615, 732
Simon, J. D., Drlica-Wagner, A., Li, T. S., et al. 2015, ApJ, 808, 95
Simon, J. D., & Geha, M. 2007, ApJ, 670, 313
Simon, J. D., Geha, M., Minor, Q. E., et al. 2011, ApJ, 733, 46
Starkenburg, E., Hill, V., Tolstoy, E., et al. 2010, A&A, 513, A34
Tollerud, E. J., Bullock, J. S., Strigari, L. E., & Willman, B. 2008, ApJ, 688, 277
Tonry, J. L., Stubbs, C. W., Lykke, K. R., et al. 2012, ApJ, 750, 99
Walker, M. G., Mateo, M., Olszewski, E. W., et al. 2015, ApJ, 808, 108
Wheeler, C., Oñorbe, J., Bullock, J. S., et al. 2015, MNRAS, 453, 1305
Willman, B., Blanton, M. R., West, A. A., et al. 2005, AJ, 129, 2692
Willman, B., Geha, M., Strader, J., et al. 2011, AJ, 142, 128
Wolf, J., Martinez, G. D., Bullock, J. S., et al. 2010, MNRAS, 406, 1220